AD-A093 454 RENSSELAER POLYTECHNIC INST TROY N Y F/G 11/6
LIQUID METAL EMBRITTLEMENT OF AMORPHOUS ALLOYS.(U)
SEP 80 N S STOLOFF, S ASHOK, M E GLICKSMAN N00014-79-C-0583
UNCLASSIFIED NL

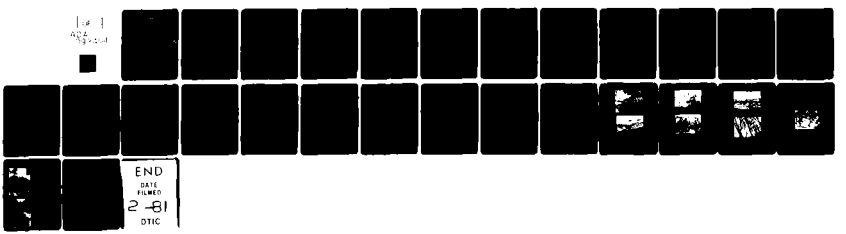

END
DATE FILMED
2-81
DTIC

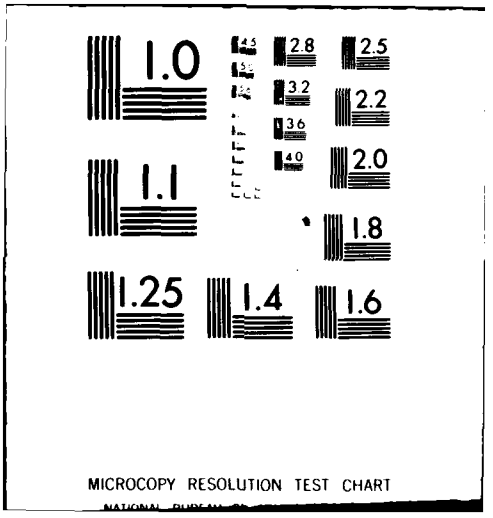
1.0
2.8
2.5
3.2
2.2
3.6
4.0
2.0
1.1
1.8
1.25
1.4
1.6
MICROCOPY RESOLUTION TEST CHART

(12)

LIQUID METAL EMBRITTLEMENT OF AMORPHOUS ALLOYS.

TECHNICAL REPORT 1 Jul 79-15 Sep 80

Submitted to:

Office of Naval Research

under

Contract No. N00014-79C9583

by

S. ASHOK, N. S. STOLOFF
M. E. GLICKSMAN and T. SLAVIN
Rensselaer Polytechnic Institute

(11) 15 Sep 1980

(10) Sankaranarayanan/Ashok
Martin E./Glicksman
Thomas/Slavin

(12) 271

Unclassified
Security Classification

DOCUMENT CONTROL DATA - R&D
(Security classification of title, body of abstract and indexing annotation must be entered when the overall report is classified)

1. ORIGINATING ACTIVITY (Corporate author)	2a. REPORT SECURITY CLASSIFICATION
Rensselaer Polytechnic Institute Troy, NY 12181	Unclassified
	2b. GROUP AD-A093 454

3. REPORT TITLE

LIQUID METAL EMBRITTLEMENT OF AMORPHOUS ALLOYS

4. DESCRIPTIVE NOTES (Type of report and inclusive dates)

Technical Report - July 1, 1979 - September 15, 1980

5. AUTHOR(S) (Last name, first name, initial)

Stoloff, Norman S., Ashok, Sankaranarayanan, Glicksman, Martin E., and Slavin, Thomas

6. REPORT DATE	7a. TOTAL NO. OF PAGES	7b. NO. OF REFS
September 15, 1980	26	14

8a. CONTRACT OR GRANT NO.	9a. ORIGINATOR'S REPORT NUMBER(S)
N00014-79C0583 new b. PROJECT NO.	
c.	9b. OTHER REPORT NO(S) (Any other numbers that may be assigned this report)
d.	

10. AVAILABILITY/LIMITATION NOTICES

None

DISTRIBUTION STATEMENT A
Approved for public release;
Distribution Unlimited

11. SUPPLEMENTARY NOTES	12. SPONSORING MILITARY ACTIVITY
None	Office of Naval Research

13. ABSTRACT

Liquid metal embrittlement of four iron-base amorphous alloys has been demonstrated by means of tensile and bend tests. Fractographic features are shown to change markedly when fracture is accomplished under liquid metals. Similarities are noted between fractographic features in liquid metals and after hydrogen charging. The results are shown to be generally consistent with a model of adsorption-enhanced shear at crack tips by embrittling agents.

DD FORM 1 JAN 64 1473

Unclassified
Security Classification

14. KEY WORDS	LINK A		LINK B		LINK C	
	ROLE	WT	ROLE	WT	ROLE	WT
amorphous						
fracture						
fractography						
shear						
liquid metals						
mercury						

INSTRUCTIONS

1. ORIGINATING ACTIVITY: Enter the name and address of the contractor, subcontractor, grantee, Department of Defense activity or other organization *(corporate author)* issuing the report.

2a. REPORT SECURITY CLASSIFICATION: Enter the overall security classification of the report. Indicate whether "Restricted Data" is included. Marking is to be in accordance with appropriate security regulations.

2b. GROUP: Automatic downgrading is specified in DoD Directive 5200.10 and Armed Forces Industrial Manual. Enter the group number. Also, when applicable, show that optional markings have been used for Group 3 and Group 4 as authorized.

3. REPORT TITLE: Enter the complete report title in all capital letters. Titles in all cases should be unclassified. If a meaningful title cannot be selected without classification, show title classification in all capitals in parenthesis immediately following the title.

4. DESCRIPTIVE NOTES: If appropriate, enter the type of report, e.g., interim, progress, summary, annual, or final. Give the inclusive dates when a specific reporting period is covered.

5. AUTHOR(S): Enter the name(s) of author(s) as shown on or in the report. Enter last name, first name, middle initial. If military, show rank and branch of service. The name of the principal author is an absolute minimum requirement.

6. REPORT DATE: Enter the date of the report as day, month, year; or month, year. If more than one date appears on the report, use date of publication.

7a. TOTAL NUMBER OF PAGES: The total page count should follow normal pagination procedures, i.e., enter the number of pages containing information.

7b. NUMBER OF REFERENCES: Enter the total number of references cited in the report.

8a. CONTRACT OR GRANT NUMBER: If appropriate, enter the applicable number of the contract or grant under which the report was written.

8b, 8c, & 8d. PROJECT NUMBER: Enter the appropriate military department identification, such as project number, subproject number, system numbers, task number, etc.

9a. ORIGINATOR'S REPORT NUMBER(S): Enter the official report number by which the document will be identified and controlled by the originating activity. This number must be unique to this report.

9b. OTHER REPORT NUMBER(S): If the report has been assigned any other report numbers *(either by the originator or by the sponsor)*, also enter this number(s).

10. AVAILABILITY/LIMITATION NOTICES: Enter any limitations on further dissemination of the report, other than those imposed by security classification, using standard statements such as:

(1) "Qualified requesters may obtain copies of this report from DDC."

(2) "Foreign announcement and dissemination of this report by DDC is not authorized."

(3) "U. S. Government agencies may obtain copies of this report directly from DDC. Other qualified DDC users shall request through _____."

(4) "U. S. military agencies may obtain copies of this report directly from DDC. Other qualified users shall request through _____."

(5) "All distribution of this report is controlled. Qualified DDC users shall request through _____."

If the report has been furnished to the Office of Technical Services, Department of Commerce, for sale to the public, indicate this fact and enter the price, if known.

11. SUPPLEMENTARY NOTES: Use for additional explanatory notes.

12. SPONSORING MILITARY ACTIVITY: Enter the name of the departmental project office or laboratory sponsoring *(paying for)* the research and development. Include address.

13. ABSTRACT: Enter an abstract giving a brief and factual summary of the document indicative of the report, even though it may also appear elsewhere in the body of the technical report. If additional space is required, a continuation sheet shall be attached.

It is highly desirable that the abstract of classified reports be unclassified. Each paragraph of the abstract shall end with an indication of the military security classification of the information in the paragraph, represented as *(TS)*, *(S)*, *(C)*, or *(U)*.

There is no limitation on the length of the abstract. However, the suggested length is from 150 to 225 words.

14. KEY WORDS: Key words are technically meaningful terms or short phrases that characterize a report and may be used as index entries for cataloging the report. Key words must be selected so that no security classification is required. Identifiers, such as equipment model designation, trade name, military project code name, geographic location, may be used as key words but will be followed by an indication of technical context. The assignment of links, roles, and weights is optional.

Abstract

Liquid metal embrittlement of four iron-base amorphous alloys has been demonstrated by means of tensile and bend tests. Fractographic features are shown to change markedly when fracture is accomplished under liquid metals. Similarities are noted between fractographic features in liquid metals and after hydrogen charging. The results are shown to be generally consistent with a model of adsorption-enhanced shear at crack tips by embrittling agents.

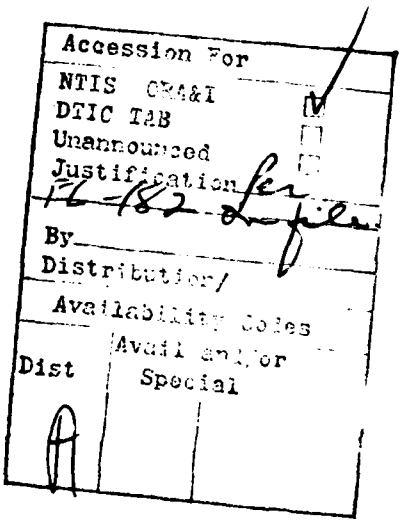

I. Introduction

During the more than 60 years that have elapsed since the discovery that mercury causes cracking of alpha brasses more than 100 combinations of solid and liquid metals have been found to constitute an embrittlement couple.[1] None of the important structural metals: steels, copper, aluminum, titanium, or nickel-base alloys are immune to this phenomenon, which often causes catastrophic failure preceded by little or no plastic deformation. In spite of the widespread occurrence of liquid metal embrittlement (LME) the field has received considerably less attention than hydrogen embrittlement (HE) or stress corrosion cracking (SCC). The phenomenon of LME does shed light on ordinary brittle fracture processes, and generally embrittlement effects are more rapidly interpretable than with other environments. Hydrogen, for example, is often liberated under stress corrosion conditions in aqueous media, and can be difficult to detect, and therefore the underlying nature of the embrittlement may be obscured.

The basic conditions that favor LME are well known. Important microstructural variables include grain size, presence of precipitates and planarity of slip, while significant test variables include test temperature, strain rate and notch acuity.[2] Chemisorption of liquid (or solid) metal atoms at a crack tip, leading to a lowering of cohesion, has been widely accepted as the embrittlement mechanism.[3,4] Recently, however, it has been suggested, based in part upon detailed fractographic observations of liquid-metal induced fractures of cadmium, aluminum alloys and steels, that LME (and perhaps HE as well) are manifestations of adsorption-enhanced localized shear, which leads to fracture at low macroscopic strains.[5,6] Considerable evidence of slip band formation at crack tips and details of fractographic features support this mechanism, which would necessitate liquid metal-induced lowering of the shear modulus.

Whatever the precise mechanism of bond-strength lowering, either in tension or in shear, the role of crystal structure in LME has always seemed to be predominant. For example, transcrystalline fracture in the presence of liquid metals has been noted for the hcp metals zinc and cadmium, wetted by mercury and gallium respectively, while fractures are generally intergranular in polycrystalline fcc metals; in the case of steels, and binary ferrous alloys, transgranular failures have been noted in most cases, although cleavage has not been reported.

The purpose of the present work was to determine whether LME occurs in amorphous metals, and if so, the mechanism of such embrittlement. Perhaps the most vexing aspect of all previous studies of LME and solid-metal induced embrittlement (SMIE) has been the inability to identify the specific atomic or electronic interaction between environment and substrate that results in reduced cohesion or enhanced shear and thereby produces embrittlement. Embrittlement of a non-crystalline metal would force attention to be focussed upon this most fundamental of all questions involving LME, while permitting the controlled introduction of crystal structure considerations through thermal treatments. Since amorphous alloys yield and fracture in air through shear processes, this class of materials should offer a particularly sensitive test of the concept of enhanced shear. Moreover, amorphous alloys of transition metals of differing d shell occupancy can be used in embrittlement studies in order to assess the role of electronic structure on fracture behavior. Such an approach has already been used to explain differences in ductility among various glassy alloys.[7]

Materials Studied

Four amorphous alloys, (1) $Fe_{81.5}B_{14.5}Si_4$, (2) $Fe_{81.5}B_{13.5}Si_{2.5}C_{2.5}$, (3) $Fe_{40}Ni_{40}P_{14}B_6$ (MetGlas 2826), and (4) $Fe_{40}Ni_{38}B_{18}Mo_4$ (MetGlas 2826 MB), were chosen for the study of the effect of liquid metal environments on their

mechanical properties. The first two alloys were supplied by General Electric Co., and the latter two were purchased from Allied Chemical Corporation.

Experimental Procedure

The FeCBSi and FeBSi were initially tested, without reduced gauge sections, in air and in a Hg-In environment. Hg-In was chosen rather than Hg to facilitate wetting. The liquid alloy was applied to the specimen using a solder iron, with dilute HCl present as a flux. A few tests were performed to see whether the heating due to the iron or the flux affected the results and no effect was found. The results from the tests with no gauge sections are summarized in Table 1.

When testing, even with great precautions, fracture often occurred at the grips. Hence, subsequent tests were performed with specimens with reduced gauge sections. The specimens, see Fig. 1, were shaped with a Tensilgrind machine; edges were polished with No. 600 emery paper. The specimens varied slightly in width and many times fracture did not occur at the minimum cross-section. Hence, the width of the specimen at the fracture surface was measured using a traveling microscope. As no reduction in width during testing occurred, there is no error in measurement. In each condition ten specimens were tested and averages of all data were determined. The tensile tests were performed in a MTS table-model tensile machine. Aluminum shims were used to enhance friction in the grips. Room and elevated temperature tests were carried out either in air or under liquid metal. Liquid Hg-In was removed with sulfur from fracture surfaces, after test in order to allow observation of fractographic features in the SEM. Bend tests also were performed, following the procedure of Luborsky and Walter.[8] In this method, ductility is determined by measuring the radius of curvature at which fracture occurs in a simple bend test between parallel plates. The strain required for fracture, $\lambda_f = t/(2r_f - t)$ where r_f is the separation of the plates at fracture and t = specimen thickness.

Results

Representative tensile stress-strain curves are shown in Fig. 2. The latter were linear for all four alloys in both air and in liquid metal at 25°C. As is typical of amorphous alloys, samples exhibited no work hardening and, upon reaching the yield stress, catastrophic fracture occurred. Hence, the only data which can be compared in the various environments are fracture stress and elastic modulus. Moduli apparently were unaffected by the liquid metal. However, liquid metal drastically affected the fracture strength and Tables 2 and 3 summarize the results for FeBCSi and FeBSi, respectively. The effect of liquid metal on Metglases, summarized in Table 1, is less severe than on the GE alloys. This possibly is due to silicon present in the GE alloys. In fact, the strength of FeBSi, which has the higher silicon content, is reduced the most of all alloys tested.

The fracture surfaces of the GE alloys were observed by SEM. Characteristic veining patterns were noted on samples tested in air, as shown in Fig. 3 a). When the alloys were tested in liquid metal the fracture appearances at low magnification are very different, as shown in Fig. 3 b). Note the small, flat facets on the surface.

In order to examine the effectiveness of liquid metals as embrittlers in the presence of plastic deformation, the GE alloys were tested at 100°C and 200°C in air and in liquid metals. Tables 2 and 3 also list these results, and it can be seen clearly that the strength does not decrease in Hg-In at 100°C as much as at room temperature. The same behavior is sometimes noted with crystalline alloys tested at elevated temperatures.

The strength reduction due to Pb-Sn solder at 200°C in the case of FeBSiC is moderate but, surprisingly, the strength in liquid metal seems to improve (from 1.451 to 1.684 GPa) in the case of FeBSi. This is being investigated further.

An interesting point in Table 2 to note is that the strength of FeBSiC in air seems to increase with increasing temperature, which may be due to the alloy becoming ductile with increasing temperature. (At 300°C in air the tensile ductility is 8.98%.) This also is the subject of future work.

To compare the properties of the alloys in the amorphous and crystalline states, the GE alloys were annealed at 800°C for 1/2 hour in a vacuum furnace. The results from testing the crystallized specimens of FeBCSi and FeBSi in air and in Hg-In at room temperature are given in Table 4. Crystallizing the alloy decreases the strength and the effect of liquid metal is limited. The fracture surfaces [Figs. 4 a) and 4 b)] clearly show that in both air and in liquid metal fracture is intergranular. This type of fracture may be due to segregation of B to grain boundaries. Since the alloys are already embrittled by such segregation, the effect of the liquid metal is less severe than might be noted if grain boundary segregation did not occur.

To compare LME with other types of embrittlement some specimens were tested at 25°C after aging at 250°C for 1 hour in vacuum. Another set of specimens was cathodically charged with hydrogen in a 5 wt% H_2SO_4 in water and 5 mg sodium arsenite solution. The charging was done at 1 mA/sq. cm. for 15 minutes, followed immediately by tensile testing. The results of these tests also are given in Tables 2 and 3. Fracture surface appearance, after cathodic charging, Fig. 5 a), is similar to that produced by tests in liquid metal, Fig. 3. However, at high magnifications a very fine cellular network is visible, see Fig. 5 b). A similar cellular network also has been seen in FeBSi tested in Hg-In at 25°C, see Fig. 6.

To study if these environments have any effect on ductility of amorphous alloys, bend tests were used. The shiny side of each specimen was placed in tension. Table 5 shows the bend ductility of the GE alloys. The fractured

specimens were observed in the SEM. Fig. 7 shows the shear zone ahead of the crack after tests in various environments. In air the shear bands are wavy, while in Hg-In and after charging with H_2 the bands are straight. The size of the plastic zone, however, is approximately the same in each of the cited cases. The plastic zone size is, on the other hand, nearly halved by the aging process. This indicates that the mechanism of embrittlement due to aging possibly is different than that responsible for HE or LME. A quantitative analysis of the shear band spacing and height are being carried out in an effort to resolve this question.

Discussion

The present work demonstrates, for the first time, that amorphous metal alloys can be embrittled by liquid metals. Embrittlement was demonstrated in three ways: loss of fracture strength, loss of bend ductility, and change in appearance of fractographic features. The tensile strengths measured for the test alloys in air, incidentally, are in good agreement with previously published values.[9,10]

The generally accepted mechanism of liquid metal embrittlement of crystalline metals is adsorption-induced lowering of bond strength, i.e. a decohesion model, as shown schematically in Fig. 8.[3] The importance of adsorption to this model, as a means of bringing embrittler atoms into contact with the base metal, has never been seriously questioned; rather, attention has been directed towards possible means by which bond strength is lowered once atoms of the embrittler are in contact with the substrate at the crack tip. Unfortunately, there has been no progress in this regard either with LME or in the closely related problem of hydrogen embrittlement. The nature of the interaction between liquid (or hydrogen) and solid, therefore, remains unknown. This has not precluded widespread studies of the effects of metallurgical test variables on LME.

Recently, there have been several reports by Lynch and co-workers[5,6] of fractographic features on liquid metal-embrittled alloys which are indicative of considerable plastic deformation accompanying fracture. Crystallographic analyses of crack paths in embrittled samples, metallographic evidence for extensive slip at crack tips and occurrence of "dimples" as the predominant fractographic features have been the basis of an adsorption-induced plasticity model, schematically shown in Fig. 9.[6] On this model the role of the embrittler is to facilitate nucleation of slip dislocations, such that plasticity is concentrated in narrow zones at the crack tip. The intense shear generated as a result of adsorption is then pictured as leading to an apparently "brittle" (i.e. little macroscopic plastic deformation) fracture. On a microscopic scale, however, shear is extensive and fracture is plastically induced.

The role of grain boundaries in embrittlement of crystalline metals is to provide barriers to plastic deformation, and in some cases (fcc metals) to serve as a low-energy crack path. Dislocations moving on slip planes pile-up at grain boundaries (or sub-boundaries in the case of single crystals) and exert a stress concentration sufficient to nucleate a crack in the presence of liquid metal. In the case of amorphous metals, there are no grain boundaries, and the concept of crystallographic slip planes does not exist. Nevertheless, plastic deformation does occur by intense homogeneous shear on planes or surfaces inclined at about 45° to the stress axis. Since strain hardening does not occur in amorphous solids (deformation is accomplished by quasi-viscous flow), the initiation of shear along a single band in a tensile test leads to fracture of the specimen at the yield stress. Macroscopic strains under such conditions are very small, although localized shear strain is extensive, of the order of 10 or more.

The veining patterns displayed by fractured metallic glasses have been

the subject of intense speculation. Masumoto and Maddin,[11] in reviewing a number of reports of such patterns, suggested that they are inherent properties of amorphous solids. Apparently, the vein zone is produced by a combination of shear with a tension component. The vein pattern may, therefore, be caused by initiation and subsequent joining of small cracks or voids. Takayama and Maddin[12] later observed slow crack growth in $Ni_{55}Pd_{35}P_{10}$ and showed that cracks initially grow in a stable manner with increasing stress, after plastic zones form ahead of the crack. Crack growth in this stage was observed to proceed by void link-up with the crack tip, while subsequent unstable crack growth seemed to proceed with the aid of adiabatic heating induced by high strain rate deformation.

The fractographic features produced by LME or HE, on the other hand, are much different. Small flat facets, interspersed with cleavage-like river markings are quite apparent, as shown in Fig. 3 b) for LME and in Fig. 5 for HE. Lynch has previously reported similarities in fractographic features produced by liquid metal and hydrogen environments in crystalline metallic alloys such as Al-base alloys and D6Ac steel.[5]

Nagumo and Takashi[13] have previously reported hydrogen embrittlement in cathodically charged $Fe_{80}P_{13}C_7$ and $Fe_{70}Cr_{10}P_{13}C_7$ amorphous alloys. Accompanying embrittlement was a change in fracture plane orientation relative to the tensile axis from 45° in as-quenched samples to 90° for hydrogen-charged ones. Fractographic features of as-quenched foils exhibited the characteristic veining pattern, while hydrogen charged foils showed a cellular pattern with large ridges. The present investigation similarly showed a distinct change in fracture morphology with hydrogen charging, although flat facets rather than a cellular pattern were observed at low magnification, Fig. 5 a). At high magnification, however, a cellular pattern was seen, Fig. 5 b).

The present work, together with earlier observations of hydrogen embrittlement in amorphous alloys,[13,14] are generally consistent with the enhanced shear mechanisms proposed by Lynch.[5,6] Since fracture in these solids, when tested in air, proceeds by intense shear with no macroscopic ductility, the decohesion model does not apply. Fracture, in other words, occurs by shearing bonds beyond their breaking strength, rather than by exerting normal stresses across the fracture plane.

Therefore, it is reasonable to assume that "normal" fracture processes in metallic glasses are accentuated by the adsorption of hydrogen or appropriate liquid metal atoms. The present work has not yet established whether shear bands are increased in number or intensity at the crack tip by these environments. However, the morphology of these bands certainly is altered. Further work is being carried out to measure quantitatively these morphological changes.

Summary and Conclusions

Liquid metal embrittlement of several amorphous glasses has been demonstrated. Fractographic features in embrittled samples are much different from those in samples fractured in air, and in fact closely resemble features noted in hydrogen embrittled samples. Embrittlement produced by heat treatment leads to somewhat different fractographic features and a smaller plastic zone, suggesting the possibility of a different mechanism of embrittlement.

It is tentatively concluded that liquid metal embrittlement and hydrogen embrittlement of amorphous metals are a consequence of enhanced shear at crack tips.

References

1. F. A. Shunk and W. R. Warke, Scripta Met., V. 8, 1974, p. 519.

2. N. S. Stoloff, in Surfaces and Interfaces, V. II, Syracuse Univ. Press, 1968, p. 157.

3. N. S. Stoloff and T. C. Johnson, Acta Met., V. 11, 1963, p. 251.

4. A. R. C. Westwood and M. H. Kamdar, Phil. Mag., V. 8, 1963, p. 787.

5. S. P. Lynch, Mechanisms of Environment-Sensitive Cracking of Materials, The Metals Society, London, 1977, p. 201.

6. S. P. Lynch, Scripta Met., V. 13, 1979, p. 1051.

7. H. S. Chen, Mat. Sci. and Eng., V. 26, 1976, p. 79.

8. F. E. Luborsky and J. L. Walter, J. Appl. Phys., V. 47, 1976, p. 3648.

9. L. A. Davis, Scripta Met., V. 9, 1975, p. 431.

10. L. A. Davis, C. P. Chou, L. E. Tanner and R. Ray, Scripta Met., V. 10, 1976, p. 937.

11. T. Masumoto and R. Maddin, Mat. Sci. and Eng., V. 19, 1975, p. 1.

12. S. Takayama and R. Maddin, Mat. Sci. and Eng., V. 23, 1976, p. 261.

13. M. Nagumo and T. Takahashi, Mat. Sci. and Eng., V. 23, 1976, p. 257.

14. A. Kawashima, K. Hashimoto and T. Masumoto, Scripta Met., V. 14, 1980, p. 41.

Table 1

Embrittlement of Amorphous Alloys at 25°C

Alloy	σ_F (GPa)		
	air	Hg	Hg-In
$Fe_{81.5}B_{14.5}Si_4$	1.90 ± 0.26	1.36 ± 0.4	1.26 ± 0.33
$Fe_{81.5}B_{13.5}Si_{2.5}C_{2.5}$	1.50 ± 0.37	—	1.03 ± 0.48
$Fe_{40}Ni_{40}P_{14}B_6$ (2826)	1.30 ± 0.21	—	1.18 ± 0.16
$Fe_{40}Ni_{38}B_{18}Mo_4$ (2826 MB)	1.60 ± 0.19	—	1.48 ± 0.17

Table 2

Effect of Environment on Fracture Strength of FeBCSi

Test Condition / Temperature °C	air	H_2	Hg-In	$Sn_{60}Pb_{40}$	Aged 250°C, 1 hour test in air
			(GPa)		
25	1.50	0.33	1.03	—	1.24
100	1.63	—	1.62	—	—
200	2.20	—	—	1.83	—
300	1.47	—	—	—	—

Table 3

Effect of Environment on Fracture Strength of FeBSi

Test Condition / Temperature °C	air	H_2	Hg	Hg-In	$Sn_{60}Pb_{40}$	Aged 250°C, 1 hour test in air
				(GPa)		
25	1.90	0.72	1.36	1.24	—	1.63
100	1.65	—	—	1.56	—	—
200	1.45	—	—	—	1.68	—

Table 4

Tensile Strengths of Alloys Crystallized at 800°C

Alloy	Environment	UTS (GPa)
FeBCSi	air	1.06
FeBCSi	Hg-In	0.94
FeBSi	air	0.88
FeBSi	Hg-In	0.74

Table 5

Bend Ductility, 25°C

Condition	FeBSiC	FeSiB
Air	0.024	Does not fracture
Hg-In	0.010	0.246
H_2 Charged	0.008	—
Aged	0.018	—

FIGURE CAPTIONS

Fig. 1 Tensile specimen configuration.

Fig. 2 Stress-strain curves for FeBCSi tested in air.

Fig. 3 Fractographs of FeCBSi, tested in tension at 25°C.
(a) air
(b) Hg-In.

Fig. 4 Fractographs of FeSiB tested at 25°C after crystallization heat treatment at 800°C.
(a) air
(b) Hg-In.

Fig. 5 Fractographs of FeBSi tested at 25°C in air after cathodic charging.
(a) flat facets at low magnification
(b) cell pattern at high magnification.

Fig. 6 High magnification fractograph of FeBSi tested at 25°C in Hg-In; compare to Fig. 5 b).

Fig. 7 Shear zone in bend specimens of FeCBSi, 25°C.
(a) air
(b) Hg-In
(c) cathodically charged.

Fig. 8 Schematic of decohesion model, showing influence of liquid metals on bond strength, σ_m, and energy to rupture bonds, U(r).[3]

Fig. 9 Adsorption-induced plasticity model of liquid metal embrittlement.[5,6]

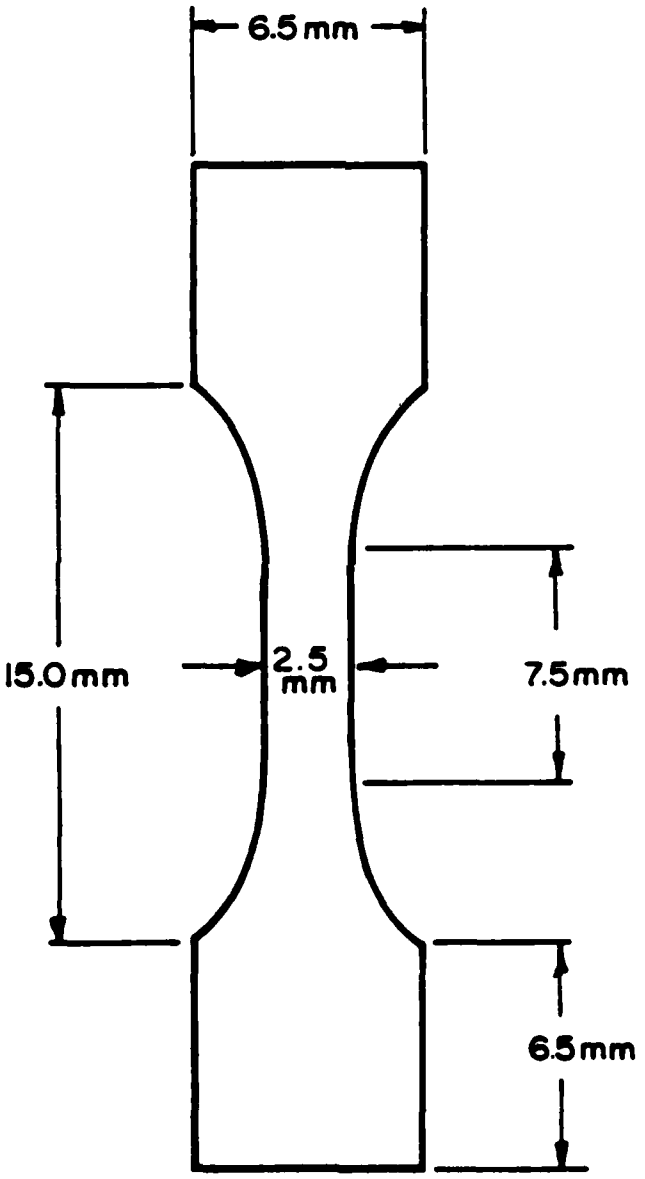

Fig. 1 Tensile specimen configuration.

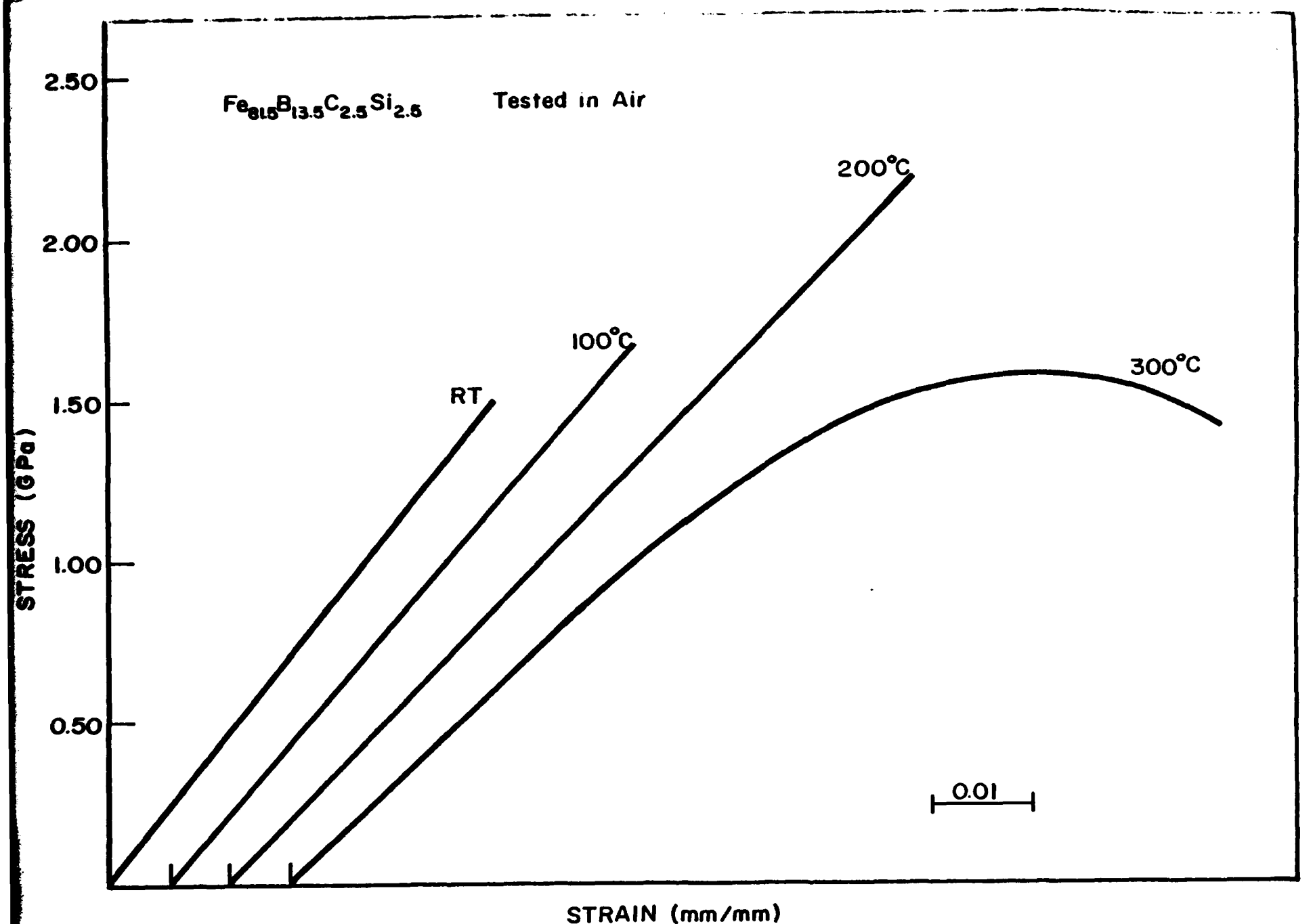

Fig. 2 Stress-strain curves for FeBCSi tested in air.

(a)

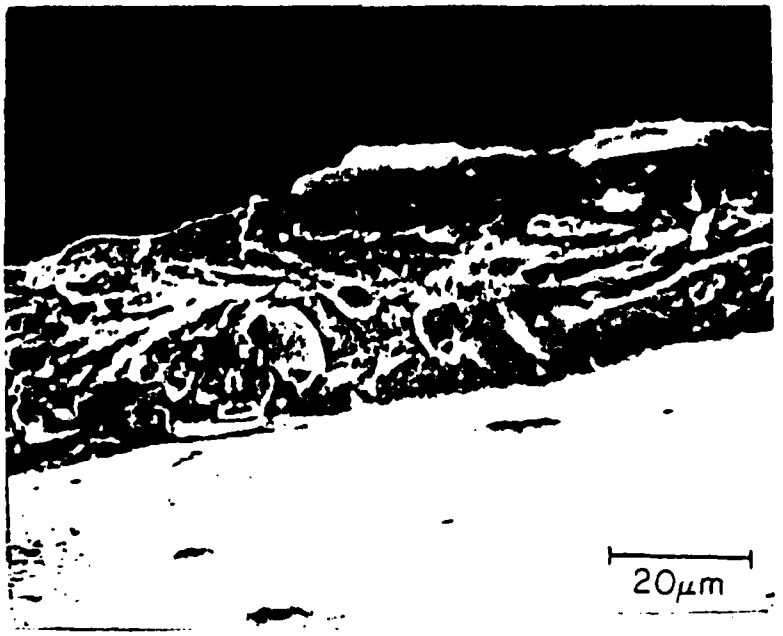

(b)

Fig. 3 Fractographs of FeCBSi, tested in tension at 25°C.
(a) air
(b) Hg-In.

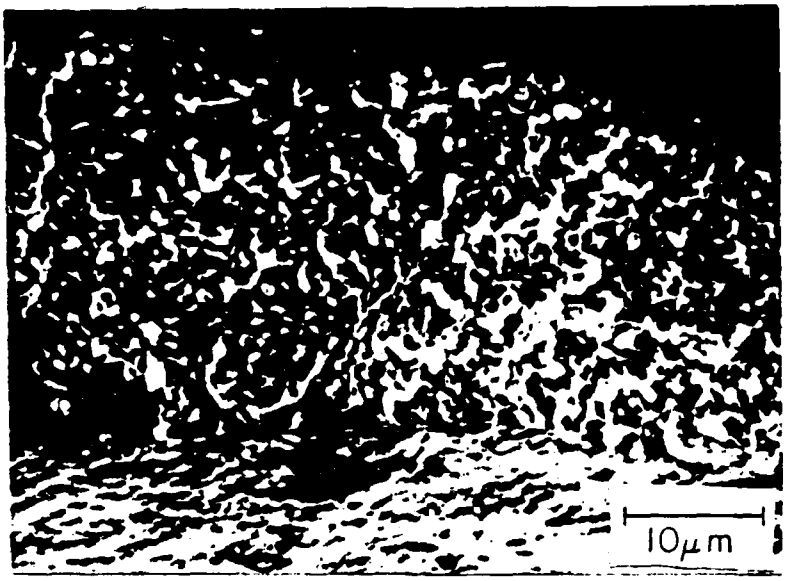

(a)

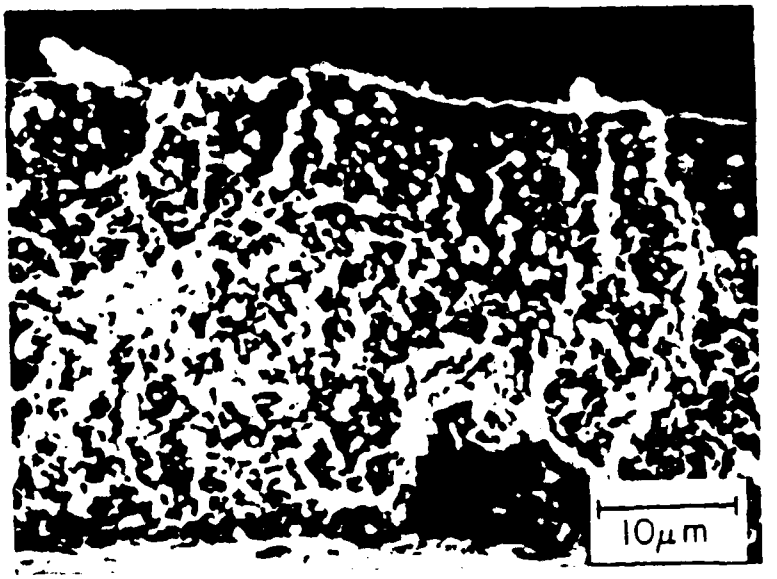

(b)

Fig. 4 Fractographs of FeSiB tested at 25°C after crystallization heat treatment at 800°C.
(a) air
(b) Hg-In.

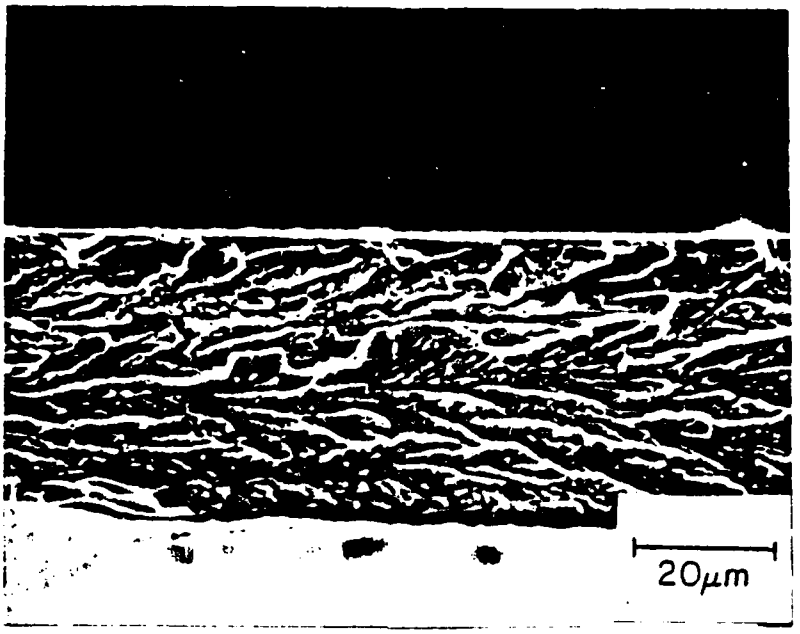

(a)

(b)

Fig. 5 Fractographs of FeBSi tested at 25°C in air after cathodic charging.
(a) flat facets at low magnification
(b) cell pattern at high magnification.

Fig. 6 High magnification fractograph of FeBSi tested at 25°C in Hg-In; compare to Fig. 5 (b).

(a)

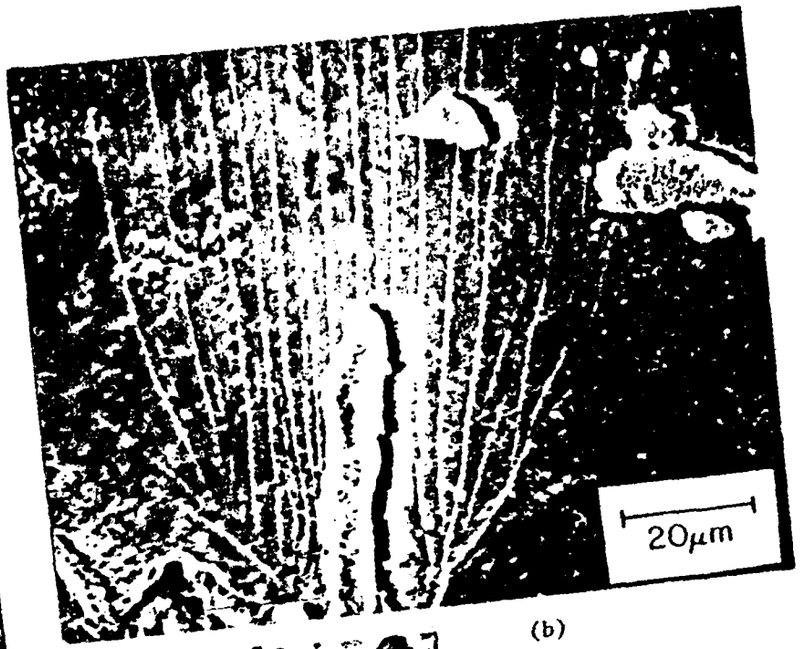

(b)

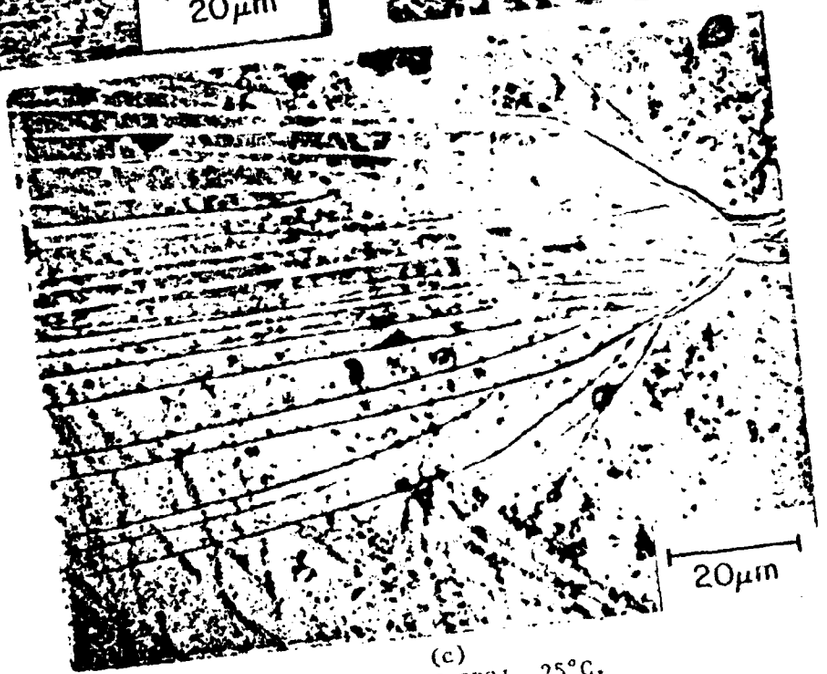

(c)

Fig. 7 Shear zone in bend specimens of FeCBSi, 25°C.
(a) air; (b) Hg-In; (c) cathodically charged.

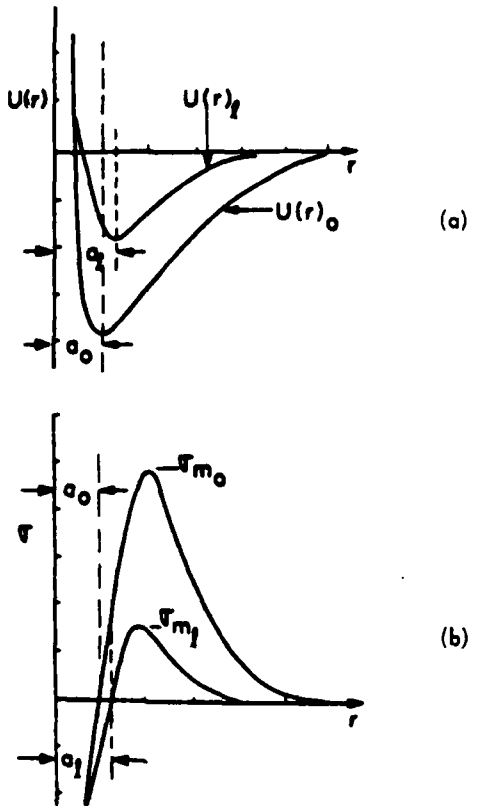

Fig. 8 Schematic of decohesion model, showing influence of liquid metals on bond strength, σ_m, and energy to rupture bonds, U(r).[3]

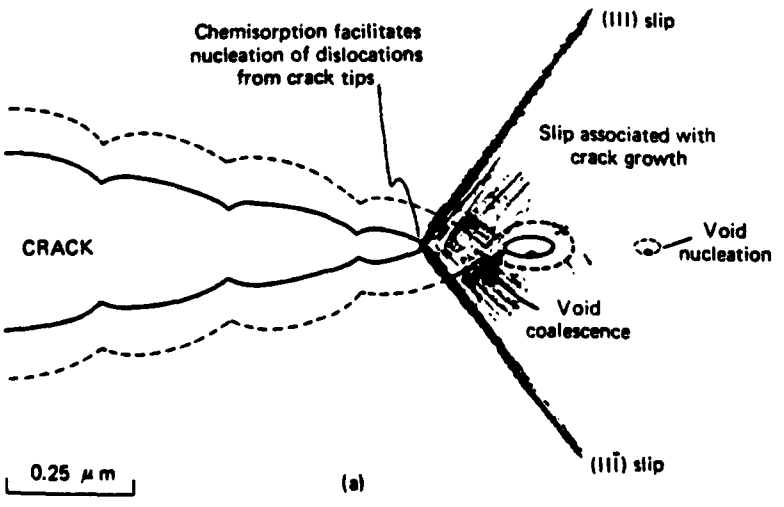

Fig. 9 Adsorption-induced plasticity model of liquid metal embrittlement.[5,6]